

Control of tensile strain and interdiffusion in Ge/Si(001) epilayers grown by molecular-beam epitaxy

T. K. P. Luong, M. T. Dau, M. A. Zrir, M. Stoffel, V. Le Thanh et al.

Citation: *J. Appl. Phys.* **114**, 083504 (2013); doi: 10.1063/1.4818945

View online: <http://dx.doi.org/10.1063/1.4818945>

View Table of Contents: <http://jap.aip.org/resource/1/JAPIAU/v114/i8>

Published by the AIP Publishing LLC.

Additional information on J. Appl. Phys.

Journal Homepage: <http://jap.aip.org/>

Journal Information: http://jap.aip.org/about/about_the_journal

Top downloads: http://jap.aip.org/features/most_downloaded

Information for Authors: <http://jap.aip.org/authors>

ADVERTISEMENT



AIP Advances

Now Indexed in Thomson Reuters Databases

Explore AIP's open access journal:

- Rapid publication
- Article-level metrics
- Post-publication rating and commenting

Control of tensile strain and interdiffusion in Ge/Si(001) epilayers grown by molecular-beam epitaxy

T. K. P. Luong,¹ M. T. Dau,¹ M. A. Zrir,¹ M. Stoffel,² V. Le Thanh,^{1,a)} M. Petit,¹ A. Ghrib,³ M. El Kurdi,³ P. Boucaud,³ H. Rinnert,² and J. Murota⁴

¹Aix-Marseille Université, CNRS CINaM-UMR 7325, F-13288 Marseille Cedex 09, France

²Université de Lorraine, Institut Jean Lamour, CNRS UMR 7198, Nancy-Université, BP 70239, 54506 Vandoeuvre-lès-Nancy Cedex, France

³Institut d'Electronique Fondamentale, CNRS UMR 8622, Université Paris-Sud, Bât. 220, 91405 Orsay, France

⁴Research Institute of Electrical Communications, Tohoku University, 2-1-1 Katahira, Aoba-ku, Sendai 980-8577, Japan

(Received 3 June 2013; accepted 5 August 2013; published online 22 August 2013)

Tensile-strained and *n*-doped Ge has emerged as a potential candidate for the realization of optoelectronic devices that are compatible with the mainstream silicon technology. Tensile-strained Ge/Si epilayers can be obtained by using the difference of thermal expansion coefficients between Ge and Si. We have combined various surface, structural, and compositional characterizations to investigate the growth mode and the strain state in Ge/Si epilayers grown by molecular-beam epitaxy. The Ge growth was carried out using a two-step approach: a low-temperature growth to produce relaxed and smooth buffer layers, which is followed by a high-temperature growth to get high quality Ge layers. The existence of a substrate temperature window from 260 to 300 °C is evidenced, which allows to completely suppress the Ge/Si Stranski-Krastanov growth. As a consequence of the high temperature growth, a tensile strain lying in the range of 0.22%–0.24% is obtained. Concerning the effect of thermal annealing, it is shown that cyclic annealing may allow increasing the tensile strain up to 0.30%. Finally, we propose an approach to use carbon adsorption to suppress Si/Ge interdiffusion, which represents one of the main obstacles to overcome in order to realize pure Ge-based optoelectronic devices. © 2013 AIP Publishing LLC. [<http://dx.doi.org/10.1063/1.4818945>]

I. INTRODUCTION

Silicon, germanium, and their alloys are the main materials that are used as active layers in microelectronics. However, due to their indirect band gap the production of optoelectronic devices, in particular light emitting devices, has been essentially based on III-V or II-VI semiconductors. Recently, it has been shown that strong optical gain can be obtained in tensile-strained and *n*-doped Ge layers and laser emission has been demonstrated under optical pumping using Ge as active layers.¹ Compared to Si or SiGe alloys, pure Ge displays unique optical properties. Indeed, the direct (Γ) valley of its conduction band is only 0.14 eV above the indirect (L) valley at room temperature while it is larger than 2 eV in Si. It has been shown that application of a tensile strain in Ge allows to reduce the energy difference between the Γ zone center valley and the indirect L valley. The tensile strain also lifts the degeneracy between heavy hole and light hole valence bands.^{2,3} On the other hand, *n*-type doping of Ge leads to a more efficient population of the zone center Γ valley and thus enhances optical recombination at the Brillouin zone center.^{4,5}

Tensile strain can be induced in Ge via several approaches: applying external mechanical stress,⁶ growing Ge on a larger lattice parameter substrate, such as InGaAs^{7,8}

or GeSn buffer layers,^{9,10} or by taking benefit of the thermal mismatch between Ge and Si.^{1,2,4,11–15} Among these approaches, the latter is of particular interest since it allows direct integration of Ge-based optoelectronic devices into the mainstream Si technology. However, due to the existence of a misfit as high as 4.2% between Ge and Si, it is crucial to control both the crystalline quality and the surface roughness of the Ge epilayers. Indeed, the growth of Ge on Si is considered as a typical example of the Stranski-Krastanov (SK) mode: a two-dimensional (2D) wetting layer is formed only for film thicknesses below a critical thickness of some monolayers (ML) thick, beyond which a transition to a three-dimensional (3D) islanding growth mode occurs to relieve the built-in strain in the Ge layers.^{16,17} As a result of the plastic strain relaxation, Ge films with larger thicknesses display a high density of threading dislocations and a rough surface. To prevent 3D nucleation of Ge islands, a two-step growth technique has been proposed, which consists of a low-temperature growth to form a strain-relaxed layer, followed by a growth at higher temperatures to produce thicker films.^{18,19} This growth technique has proven its efficiency regarding the reduction of the density of threading dislocations and also the surface roughness.^{1,2,4,11,12,20,21} However, it is worth noting that in all above-mentioned experiences, the chemical-vapor deposition (CVD) technique has been exclusively used. While the low-temperature growth step is recognized to be crucial to control the final state of the film

^{a)}Email: lethanh@cinam.univ.mrs.fr

crystalline quality, the degree of freedom regarding the choice of the substrate temperature remains limited within the CVD technique. Indeed, in a standard CVD process, the thermal energy provided by the substrate temperature should be high enough to dissociate the gas precursor molecules.^{22,23} For this reason, in previous works the low-temperature step has been indeed carried out at intermediate temperatures ranging between 350 and 400 °C.^{1,2,4,11,12,20,21} In addition, the presence of hydrogen on the growing surface that comes from hydrogen carrier gas or decomposition of hydride molecules may lower the surface diffusion length of Ge adatoms.²⁴ For example, it has been shown that Ge films grown by CVD at a temperature reduced down to 330 °C present a high density of stacking faults and defects.²⁵

In this work, we report results of controlling tensile strain in Ge epilayers grown on Si(001) substrates using molecular-beam epitaxy (MBE). One of the advantages of the MBE technique is that it does not need high growth temperatures to dissociate gas precursors. Ge films were grown using a two-step procedure. Concerning the growth of the first Ge layer, our purpose aims to determine growth conditions that allow getting strain-relaxed and smooth Ge layers. We have then investigated, in the first set of experiments, the Ge growth mode as a function of the growth temperature within a wide temperature range going from room temperature up to 550 °C. We have evidenced the existence of a narrow substrate temperature window, from 260 to 300 °C, in which the Stranski-Krastanov growth of Ge on Si can be completely suppressed. Instead, a two-dimensional growth mode is obtained up to film thicknesses larger than 200 nm. The resulting Ge epilayers are shown to be almost free of threading dislocations. In the second set of experiments, we have investigated the effect of parameters, such as growth temperature, film thickness, and annealing condition on the strain level of Ge epilayers. It is shown that Si/Ge interdiffusion, in particular the upward diffusion of Si into the deposited Ge layer is a challenge to overcome in order to envisage the fabrication of Ge-based optoelectronic devices. Finally, we propose an approach to use stacked layers of carbon/germanium near the interface region to suppress Si/Ge interdiffusion.

II. EXPERIMENTAL

Ge growth was performed in a standard solid source MBE system with a base pressure better than 5×10^{-10} millibars. The growth chamber is equipped with a 30-keV reflection high-energy electron diffraction (RHEED) apparatus allowing monitoring in *real time* the Ge growth mode. An Auger electron spectrometer (AES) is used to control the cleanliness of the substrate surface prior to growth and the film composition. Ge was evaporated from a two-zone heated Knudsen effusion cell to avoid Ge condensation at the upper part of the cell crucible, thus insuring a highly stable Ge deposition rate. The Ge deposition rate, measured using RHEED intensity oscillations during Ge homoepitaxy on a Ge(111) substrate, was in the range from 1.5 to 5 nm/min. Carbon evaporation was carried out using a sublimation source of high-purity pyrolytic graphite and the carbon flux was estimated based on the change of the surface reconstructions

from (2×1) to $c(4 \times 4)$ upon carbon adsorption on a Si(001) surface.²⁶

The substrates were flat, *p*-type Si(001) wafers. Cleaning of the substrate surface followed the hydrogen-terminated Si(001) method, which consists of two steps: the first is a wet chemical treatment in NH_4F solution to prepare an ideally SiH_2 -terminated Si(001) surface.²⁷ The second step is an annealing in ultrahigh vacuum to desorb the passivating hydrogen layer at a temperature of about 500 °C. After this step, the Si surface exhibits a well-developed 2×1 reconstruction and AES measurements do not reveal any presence of oxygen or carbon. The substrate temperature was measured using a thermocouple in contact with the backside of Si wafers. These measurements were corrected using an infrared pyrometer (Iron, W-series) operating in the wavelength region of 0.90–1.08 μm , in which the emissivity of Si is constant. The accuracy of the temperature measurement is estimated to be about ± 20 °C.

Structural analysis of post-grown films was performed by means of high-resolution transmission electron microscopy (HRTEM) using a JEOL 3010 microscope operating at 300 kV with a spatial resolution of 1.7 Å. The strain level in the Ge epilayers was deduced from X-ray diffraction (XRD) measurements performed using a diffractometer (Philips X'pert MPD) equipped with a copper target for $\text{Cu-K}_{\alpha 1}$ radiation ($\lambda = 1.54059$ Å). The angular resolution is $\sim 0.01^\circ$. The Ge and Si profiles were measured by secondary ion mass spectrometry (SIMS), using Cs^+ primary ion beams at 1 kV impact energy and with an incidence angle of about 68.4° from the normal of the sample surface. The primary beam intensity and the raster area were set at 42 nA and $200 \times 200 \mu\text{m}^2$, respectively. To improve the spectrometer transmission, we used a contrast of 400 μm and a field aperture of 750 μm to decrease aberrations. The depth calibration was performed using crater Alpha-step depth measurement.

III. RESULTS AND DISCUSSION

This section will be divided into 3 subsections in which we present results concerning the Ge growth using the two-step growth technique, the effect of annealing parameters on the tensile strain level in the Ge epilayers and finally the Si/Ge interdiffusion and an approach to suppress interdiffusion.

A. Two-step growth of Ge

One of the direct consequences of the strain relaxation process in a Stranski-Krastanov growth system is that the epilayers present a high density of threading dislocations and a rough surface. Fig. 1 displays typical TEM images of a ~ 650 nm thick Ge film deposited on a Si(001) substrate at a constant temperature of 730 °C. The overall view of the Ge layer (Fig. 1(a)) reveals an extremely rough surface and interface. The misfit dislocation network located at the interface region is so dense that the interface between the Ge overlayer and the substrate is very poorly defined. Fig. 1(b) shows that the defected region is extended to more than 200 nm thick and deeply penetrates into the substrate. Atomic Force Microscopy (AFM) measurements of the film surface morphology indicate an average roughness higher

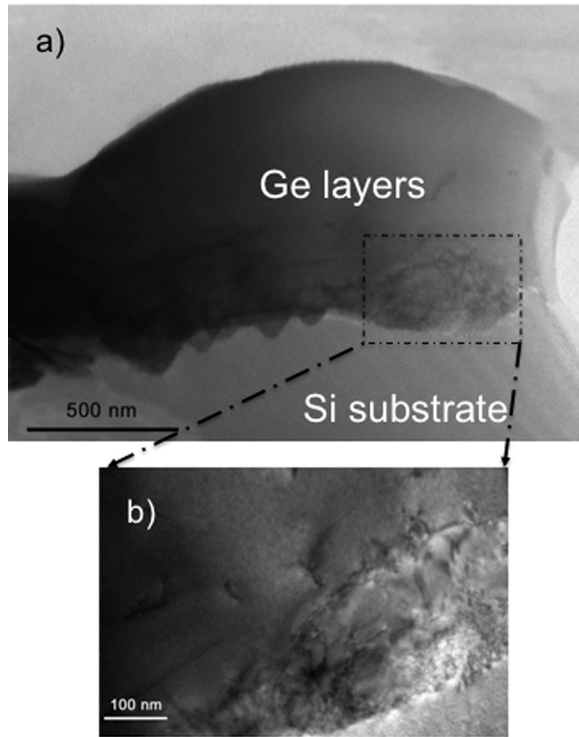


FIG. 1. (a) Typical TEM image of a ~ 650 nm thick Ge film deposited on a Si(001) substrate at a constant temperature of 730°C ; (b) A zoom taken near the interface region, illustrating the extension of the defected region to more than 200 nm thick.

than 80 nm. This high surface roughness unambiguously results from the growth mode transition from 2D to islanding growth. We note that threading dislocations across the Ge layer are not visible from the above cross-sectional TEM image, which is probably due to a too high thickness of the prepared sample. To improve the crystalline quality and the surface roughness of Ge/Si films, compositionally graded SiGe buffered layers with a gradually increased Ge concentration are traditionally used.²⁸ These buffered layers have generally thicknesses of up to some μm . Regarding the two-step growth technique, efforts are focused on the control of the strain state and the film surface morphology at low

temperatures, thus in general a Ge layer of only a few dozens of nm thickness is needed. For a standard MBE growth rate of some nm per min, the key feature of the low-temperature step relies on the choice of the growth temperature, and hence the surface diffusion length of adatoms, in order to control the Ge growth mode transition.

The RHEED technique, thanks to the grazing incidence of the electron beam, allows one to monitor in *real-time* the evolution of the film surface morphology and structure. Indeed, it is now well established that the 2D growth regime is associated with the observation of *streaky* RHEED patterns due to electron diffraction from a smooth surface, while 3D growth is characterized by *spotty* patterns due to transmission diffraction through 3D islands. We have then used RHEED to investigate the Ge growth in a large temperature range, going from room temperature up to 550°C , in order to determine adequate growth conditions for the first growth step. For a growth temperature below 150°C , the Ge layer becomes amorphous after deposition of a certain thickness, from a few to a dozen nm, inversely depending on the growth temperature. In the temperature range of 150 – 550°C , as expected, the Ge growth proceeds via the SK growth mode, a 2D wetting layer (WL) is formed only for a deposited Ge thickness below 1 nm, beyond which 3D islanding nucleation occurs. Fig. 2 shows typical RHEED patterns corresponding to these two growth regimes: during the formation of the WL, a streaky pattern is observed (Fig. 2(a)), indicating that the WL surface is relatively smooth. The islanding growth mode is associated with a spotty pattern, as shown in Fig. 2(b). The fact that all 3D spots are located along (1×1) streaks indicates that they arise from a bulk diffraction effect and that islands are epitaxial.

A result of particular interest is that by carefully analyzing the Ge growth mode as a function of the substrate temperature, we have evidenced the existence of a very narrow window of temperatures, from 260 to about 300°C , in which the SK growth mode can be completely suppressed. Two-dimensional RHEED patterns are continuously observed from the first layer up to a film thickness of a few hundreds nm. Figs. 3(a) and 3(b) display RHEED patterns taken along the two main $[100]$ and $[1-10]$ azimuths of a ~ 200 nm thick

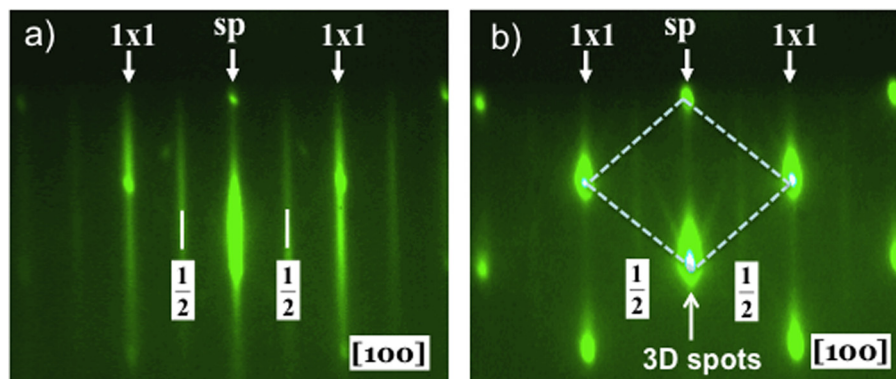


FIG. 2. RHEED patterns taken along the $[100]$ azimuth illustrating the growth mode transition in the Ge/Si system when increasing the film thickness. sp indicates the specular or (00) streaks, (1×1) corresponds to the position of the Ge bulk-like streaks and $\frac{1}{2}$ the half-order streaks of the Ge(001) 2×1 reconstructed surface; (a) streaky pattern observed during the formation of the wetting layer and (b) 3D pattern observed for film thicknesses larger than the critical thickness. The dotted lines represent a unit cell of the Ge(001) plane, which is parallel to the (001) plane of the Si substrate.

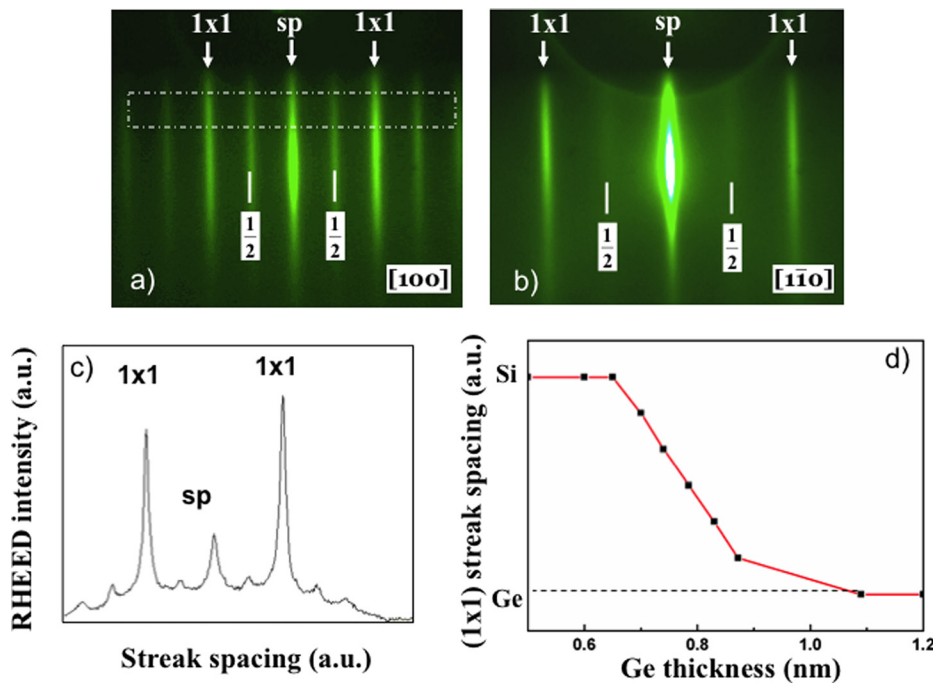


FIG. 3. (a) and (b) RHEED patterns along two main $[100]$ and $[1\bar{1}0]$ azimuths observed throughout the growth of a ~ 200 nm thick Ge layer at 300°C . The observation of long streaks in RHEED patterns clearly indicates that the formation of 3D islands has been completely suppressed; (c) Measurement of the RHEED intensity inside the rectangular region shown in (a); (d) Evolution of the (1×1) streak spacing of Ge when increasing the film thickness. The Ge epilayer is found to be fully strained up to a thickness of ~ 0.65 nm, beyond which a progressive strain relaxation takes place and a fully relaxed Ge epilayer is obtained for a thickness of ~ 1.1 nm.

Ge layer grown at a temperature of 300°C . The observation of long streaks in RHEED patterns clearly indicates that the formation of 3D islands has been completely suppressed. Analyzing the evolution of the RHEED intensity versus film thickness also allows quantifying the strain relaxation process. To do this, we first define a rectangular region, which is parallel to the RHEED pattern shadow (Fig. 3(a)), and measure the RHEED intensity profile inside this region (Fig. 3(c)) at various film thicknesses. Taking the (1×1) bulk-like streak spacing of the silicon substrate as a reference, one can either determine the Ge in-plane lattice parameter at a given thickness or follow in real-time the evolution of the relaxation process of the Ge epilayer. An example of the evolution of the (1×1) streak spacing of Ge when increasing the film thickness is depicted in Fig. 3(d). The figure reveals that the Ge epilayer is fully strained up to a thickness of ~ 0.65 nm, beyond which a progressive strain relaxation takes place and a fully strain-relaxed Ge epilayer is obtained for a film thickness of ~ 1.1 nm. This result is also confirmed by the fact that when superimposing the RHEED intensity profile of the (1×1) streak spacing of a 1.1 nm thick Ge layer together with that of the Si substrate, we find a difference of 4.2%, a value that corresponds to the misfit of the two bulk materials. It is worth noting that the above relative comparison of the streak spacing between the Ge epilayers and the Si substrate induces a much smaller error on the degree of the strain relaxation than by determining the Ge in-plane lattice parameter versus the film thickness and compare these values to that of bulk Ge. Indeed, with the same RHEED experimental set-up, the accuracy of a relative comparison of the streak spacing between two materials depends only on the measurement error of the streak spacing while the determination of the in-plane lattice parameter depends in addition on the camera length, i.e., the distance from the

point at which the incident electron beam strikes the substrate's surface to the RHEED screen.²⁹

Fig. 4 shows an overall view of a ~ 200 nm thick Ge layer grown at 300°C (Fig. 4(a)) and a zoom taken near the interface region (Fig. 4(b)). The Ge growth rate was 3.7 nm/min. In contrast to the image shown in Fig. 1(a), the overall

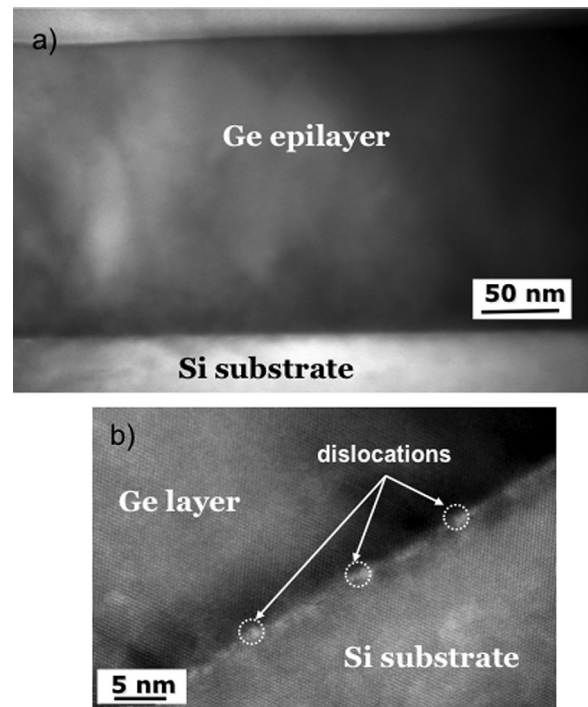


FIG. 4. (a) Cross-sectional TEM image of a 200 nm thick Ge layer grown on Si at 300°C , both the film surface and interface are relatively smooth, threading dislocations are almost absent; (b) A zoom taken near the interface region. A high density of misfit dislocations is present, which have allowed the Ge layer to be fully relaxed.

view displayed in Fig. 4(a) reveals a Ge epilayer of a high crystalline quality and a rather uniform thickness. It is worth noting that the stacking faults aligned along (111) planes, which are commonly observed in strain-relaxed Ge/Si epilayers grown at temperatures higher than $\geq 330^\circ\text{C}$ are almost absent (see, for example, Fig. 10 of Ref. 25 using CVD). Furthermore, the film surface appears relatively smooth, which is correlated with the observation of streaky RHEED patterns during Ge deposition at this temperature. A HR-TEM image taken close to the interface region (Fig. 4(b)) reveals the presence of a high density of misfit dislocations, which have allowed strain relaxation to take place in the Ge epilayer. Of particular interest, unlike the case of Ge films grown at high temperatures, for example at 370°C ,³⁰ here we observe that most of misfit dislocations are located close to the interface and only a few of them have penetrated into the Ge epilayer. This explains why the observed interface is relatively smooth and well defined.

After the low-temperature growth step, we have deposited another Ge film at higher substrate temperatures. In the following, we will consider the effect of the two-step growth process on the tensile strain in the Ge films. All samples have a total thickness of $\sim 300\text{ nm}$, which consists of a $\sim 50\text{ nm}$ thick Ge film deposited at 300°C followed by a 250 nm thick Ge layer grown at various temperatures: 400, 500, 600, 650, 700, 750, and 770°C . Fig. 5 displays some representative Ω - 2θ XRD scans taken around the Ge(004) reflection. For comparison, we report in dotted lines, a XRD scan of a sample grown at 300°C , similar to the one shown in Fig. 4. The fact that the (004) peak of the low-temperature grown sample is located at $2\theta \sim 66^\circ$, a value close to that measured on a Ge substrate, indicates that the corresponding Ge layer is almost fully relaxed. As can be seen in Fig. 5, the 2θ angle value of the (004) peak is found to linearly increase when the growth temperature increases from 300 to 700°C then remains almost constant for further increasing the temperature up to 770°C .

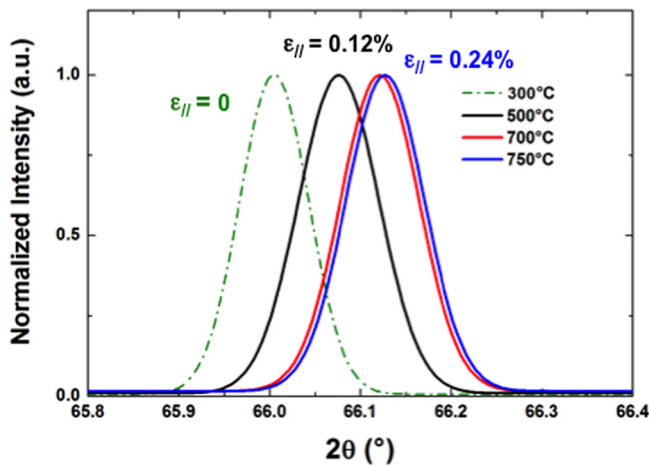


FIG. 5. Evolution of Ω - 2θ XRD scans around the Ge(004) reflection with the growth temperature. The dotted XRD scan corresponding to a sample grown at 300°C is shown for comparison. As the growth temperature increases, the Ge(004) peak linearly shifts to higher angles, reaches a saturation value at 700°C and finally remains almost constant for further increasing the temperature to 770°C . The in-plane tensile strain observed in the temperature range of 700 – 770°C is 0.24%.

TABLE I. Variation of the in-plane tensile strain in Ge films versus the growth temperature during the second step growth. All samples have a total thickness of $\sim 300\text{ nm}$, which consists of a $\sim 50\text{ nm}$ thick Ge layer deposited at 300°C followed by another 250 nm thick Ge layer grown at various temperatures: 300, 400, 500, 600, 650, 700, 750, and 770°C .

Sample's reference	Growth temperature ($^\circ\text{C}$)	In-plane tensile strain ($\epsilon_{\parallel}/\%$),
A	300	0 (full relaxation)
B	400	0.07 (± 0.01)
C	470	0.12 (± 0.01)
D	600	0.16 (± 0.01)
E	650	0.20 (± 0.01)
F	700	0.24 (± 0.01)
G	730	0.24 (± 0.01)
H	750	0.24 (± 0.01)
I	770	0.24 (± 0.01)

We note that to obtain the value of the in-plane tensile strain ϵ_{\parallel} , we first determine the out-of-plane strain ϵ_{\perp} from the Ω - 2θ XRD curves and then deduce the value of ϵ_{\parallel} using the following relationship: $\epsilon_{\parallel}/(\epsilon_{\parallel} + \epsilon_{\perp}) = c_{11}/(c_{11} + 2c_{12})$ with $c_{11} = 12.85 \times 10^{10}\text{ Pa}$ and $c_{12} = 4.83 \times 10^{10}\text{ Pa}$ for pure Ge.³¹ The highest value of the in-plane tensile strain ϵ_{\parallel} obtained in the growth temperature range of 700 – 770°C is 0.24%, which is in good agreement with previous results reported using CVD in which the highest tensile strain was in the range of 0.22%–0.25%.^{1,2,4,11,21} at similar growth temperatures. We summarize in Table I the variation of the in-plane tensile strain in Ge films versus the growth temperature during the second step growth at temperatures ranging from 300 to 770°C .

We have also investigated the effect of the film thickness on the strain state in Ge films. Fig. 6 displays XRD measurements around the Ge (004) reflection of three samples with thicknesses of 150, 450 and 600 nm. The growth temperature was chosen to be 730°C , i.e., corresponding to the substrate temperature range of 700 – 770°C in which the highest tensile strain was observed. As can be seen, the

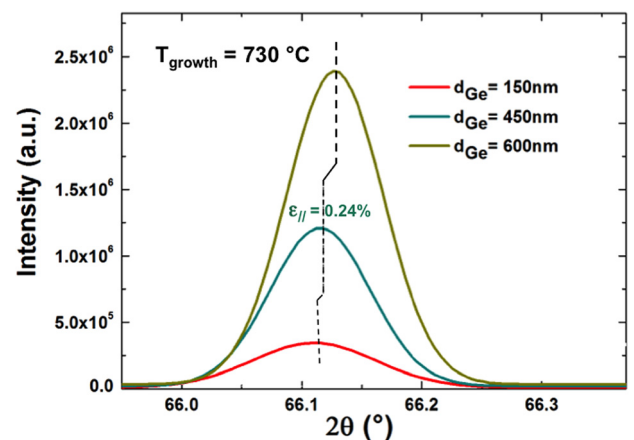


FIG. 6. Evolution of the Ge(004) peak position versus film thickness. Only a slight increase of the tensile strain ($\sim 0.01\%$) is observed when the film thickness increases from 150 to 600 nm.

position of the (004) reflection is shifted to higher angles when increasing the film thickness, indicating an enhancement of the tensile strain with the film thickness. However, it is worth noting that only a slight increase of the tensile strain, which is less than 0.01%, is observed when increasing the film thickness from 150 to 600 nm. The above result implies that regarding the value of tensile strain that can be induced in Ge epilayers, a film thickness of about 150 nm may be sufficient.

We now consider the structural properties of Ge films after the high-temperature growth step. Displayed in Fig. 7(a) is a typical TEM overall view of a sample after a growth at 730 °C. The sample consists of a ~50 nm thick Ge layer deposited at 300 °C followed by another 250 nm thick Ge layer deposited at 730 °C. We note that after the 300 °C growth step, the substrate temperature was slowly increased to 730 °C by a rate of 5 °C/min while the Ge deposition was interrupted. It is worth noting that throughout the film growth at 730 °C, the growing surface was characterized by a two-dimensional RHEED pattern, indicating that the Ge/Si SK growth at such a high temperature is also suppressed. Compared to the image of Fig. 4(a) obtained after a low-

temperature growth at 300 °C, we observe here the presence of threading dislocations (indicated by white arrows), which have been probably generated during the temperature increase to 730 °C or/and during growth at this temperature. Such an introduction of threading dislocations implies that Ge films grown at low temperatures are strain relaxed but are in a metastable state. When the temperature increases, Ge films should move to a more stable state in which both misfit and threading dislocations are introduced. However, it is worth noting that in comparison with Ge films grown by one step at a high temperature (Fig. 1), and in particular with Ge films grown by CVD (see, for example, Fig. 3 of Ref. 18 and Fig. 4 of Ref. 19), the present layer exhibits a much lower density of both misfit and threading dislocations. In addition, misfit dislocations are found to be located in the vicinity of the interface region, which result in a highly smooth interface (Fig. 7(b)).

To quantify the density of threading dislocations, we employ the selective defect-etching technique for the revelation of threading dislocations. The chromium chemical solution with the following composition was used:³² CrO₃ 0.6 mol. l⁻¹/HF 12 mol. l⁻¹/H₂O. With this Cr-based etchant, threading dislocations on the (001) surface orientation are revealed as etched pits with a square pyramidal shape. First, we optimized the etching time on a standard Ge layer grown at a high temperature in which a density of threading dislocations in the range of 10⁷ cm⁻² should be expected. In agreement with results reported in Ref. 32, it was found that the etching time in the range of 2.5–10 min is adequate for a good revelation of threading dislocations. Fig. 8(a) shows a Scanning Electron Microscopy (SEM) image after an etch of 5 min of a ~650 nm thick Ge film deposited on Si(001) at 730 °C (the TEM image of the corresponding sample is shown in Fig. 1). The density of threading dislocations is so high that a major part of them is linked to each other to form noodle-like features on the surface. In the inset of this image, we display a zoom taken inside these features. Square pyramidal pits of different sizes are clearly observed, which unambiguously indicates that those features arise from revelation of threading dislocations. We show in Fig. 8(b) a typical example of a ~300 nm Ge film grown using the two-step growth method (the TEM image of the corresponding sample is shown in Fig. 7). Interestingly, the surface exhibits a very low density of defected regions, most of them have a square shape. Inside these square-shaped regions, one can see circular regions containing a high density of square pyramidal pits that are characteristic of threading dislocations. A detailed view of a circular region is shown in the inset of the figure. If we assume that each square defected region corresponding to a *threading dislocation unit*, we obtain a defect density well below 10⁴ cm⁻², a value that is about 2–3 orders of magnitude smaller than that observed in standard samples grown by CVD.^{19–21} It is worth noting that each circular region is found to sit on crosshatch patterns, which are known to arise from a nonuniform elastic field induced by the beneath dislocations.^{33,34} Crosshatching is often observed in a low misfit system (below 2%) or when the density of threading dislocation in the relaxed film is low (<10⁶ cm⁻²). Furthermore, crosshatch lines are often oriented along the two orthogonal <110>

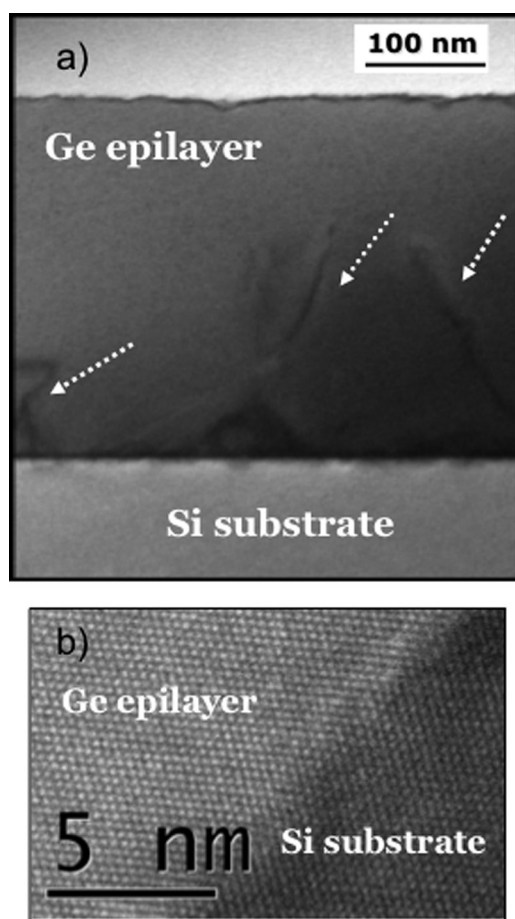


FIG. 7. (a) Typical TEM image of a ~300 nm thick Ge layer grown following a two-step growth at 300 and 730 °C. Threading dislocations, indicated by white arrows, appear in the layer during the increase to the high temperature growth step. However, the layer exhibits a low density of misfit and threading dislocations; (b) A zoom taken near the interface region, illustrating the flatness of the interface.

directions, which may explain why defected regions have a square shape.

B. Effects of thermal annealing on tensile strain

Post-growth thermal annealing has been the subject of numerous investigations; the purpose consists of reducing threading dislocations in Ge/Si heteroepilayers that are induced during growth at high temperatures.^{19,21} Thermal annealing can be done either by an anneal at a high temperature or a cyclic anneal. Since in our case, the as-grown samples already display a high crystal quality and have a low density of threading dislocation, we have focused our investigations on the effect of annealing parameters on the strain state in Ge epilayers.

We display in Fig. 9 a comparison of two annealing methods on the tensile strain: annealing at 900 °C for different durations and cyclic annealing between 780 and 900 °C with an annealing time of 10 min at each temperature. It is noted that all annealing steps were undertaken in the growth

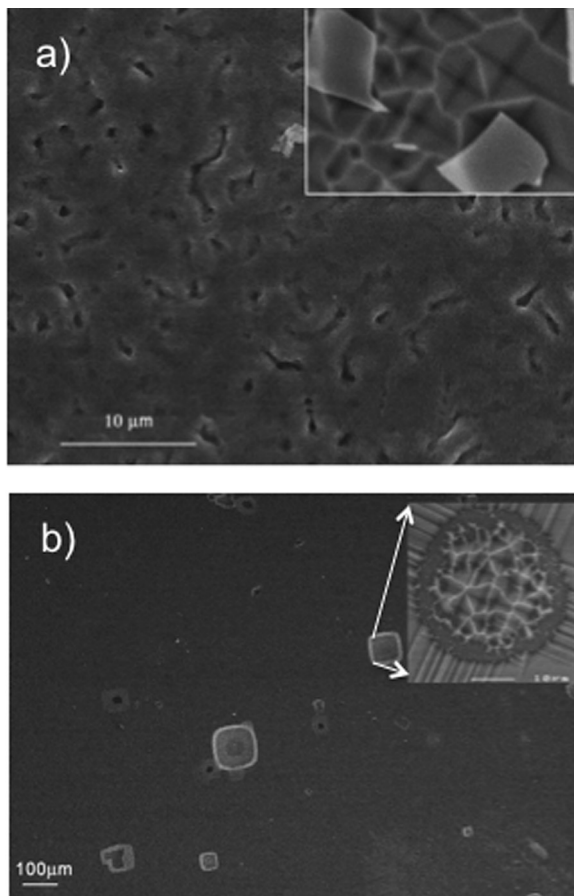


FIG. 8. SEM images of the surface after defect etching in $\text{CrO}_3/\text{HF}/\text{H}_2\text{O}$ for 5 min; (a) of a ~ 650 nm thick Ge deposited on Si(001) at 730 °C. Noodle-like features are found to be formed, which can be attributed to a high density of threading dislocations. Shown in the inset is a zoom taken inside these features. Square pyramidal pits characteristic of threading dislocations are clearly observed; (b) of a ~ 300 nm Ge layer grown using two-step growth at 300/730 °C. Defected regions having a square shape are present on the surface. In the inset, a detailed view of a square defected region is shown. If we take each square defected region as a threading dislocation unit, a defect density well below 10^4 cm^{-2} is measured.

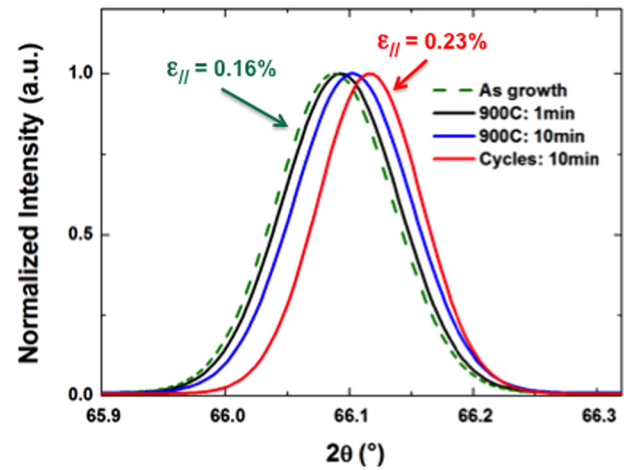


FIG. 9. Comparison of Ω - 2θ XRD scans around the Ge(004) reflection measured with annealing at 900 °C for different durations and cyclic annealing between 780 and 900 °C with an annealing time of 10 min at each temperature. The dotted scan represents the as-grown sample grown at 650 °C. Cyclic annealing is shown to generate a larger tensile strain as compared to annealing at 900 °C.

chamber just after film deposition. For comparison, we also show the (004) reflection of the as-grown sample (dotted curve). We note that for the as-grown sample, we have chosen a temperature of 600 °C during the second step growth in order to minimize further Ge/Si interdiffusion that may occur during annealing. The corresponding in-plane strain of the as-grown sample is 0.16%. For annealing at 900 °C, we have carried out five annealing times: 1, 3, 5, 7, and 10 min and display in the figure two representative (004) scans corresponding to 1 and 10 min. The in-plane strain was found to slowly increase with increasing the annealing time and reaches a value of 0.20% at $t = 10$ min. We note that for a longer annealing time, the width of the Ge(004) reflection becomes a little bit broader, suggesting that Ge/Si interdiffusion has occurred. Thus, regarding the tensile strain level, post-grown annealing at 900 °C appears to be less efficient as compared to the effect of the growth temperature. On the other hand, we find that cyclic annealing can produce a larger strain: with the same as-grown sample an in-plane strain of 0.23% can be obtained after cyclic annealing.

We have then investigated in details cyclic anneals and the following procedure was used: the samples were raised from a low temperature of 780 °C to a high temperature of 900 °C and the annealing time is kept constant at each temperature. Two sets of samples are considered, along which both the number of cycles and the annealing time are modified. First, we found that for the same annealing time, the value of strain increases when increasing the number of annealing cycles. We have thus chosen 10 annealing cycles and modified the annealing time. Fig. 10 displays XRD results with various annealing times. Two main features can be deduced from this evolution of strain versus annealing time. First, in the range of annealing times comprised between 1 and 10 min, the in-plane strain does not linearly increase with increasing the annealing time but the highest value of strain, $\varepsilon_{||} = 0.30\%$, is obtained at $t = 3$ min. To our knowledge, this value represents one of the highest values of

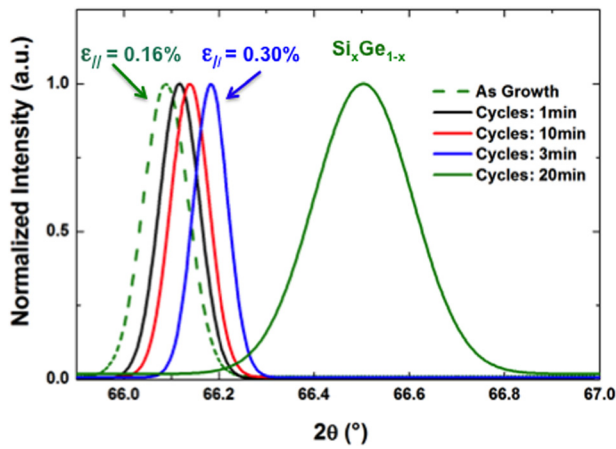


FIG. 10. Evolution of Ω - 2θ XRD scans with various annealing times during cyclic annealing. The highest tensile strain, 0.30%, is obtained for an annealing time of 3 min. For an annealing time of 20 min, the Ge(001) reflection shifts to much higher angles and at the same time its width broadens.

the tensile strain ever reported for Ge directly grown on Si. Second, for annealing times larger than 10 min, the Ge(001) reflection shifts to much higher angles and at the same time its width becomes larger. An example corresponding to an annealing time of 20 min is depicted in the figure. With the same experimental set-up, the full width at half maximum (FWHM) of the Ge(004) reflection for an annealing time below 10 min is 0.079° while it is 0.207° for the 20 min annealed sample. We note that if we use the elastic constants C_{11} and C_{12} for pure Ge, an in-plane strain up to 0.68% can be deduced, which is of course unrealistic. We summarize in Table II the variation of the in-plane tensile strain in Ge films as a function of the annealing time with two annealing methods: long anneal at 900°C and cyclic anneals between 780 and 900°C . The as-grown sample was deposited at a substrate temperature of 600°C , the corresponding in-plane tensile strain is 0.16%.

TABLE II. Variation of the in-plane tensile strain in Ge films as a function of the annealing time with two annealing methods: long anneal at 900°C and cyclic anneals between 780 and 900°C . All samples have a total thickness of ~ 300 nm, which consists of a ~ 50 nm thick Ge layer deposited at 300°C followed by another 250 nm thick Ge layer deposited at 600°C . Prior to annealing, the as-grown sample has a tensile strain of 0.16%. The highest value of the in-plane tensile strain obtained for each annealing method is shown in bold type. For cyclic anneals, the highest value of the tensile strain (0.30%) is obtained for 3 min, beyond which a decrease of the tensile strain is observed, which can be attributed to the beginning of Ge/Si interdiffusion.

Annealing condition	Annealing time (min)	In-plane tensile strain (ϵ_{ij} (%))
Long anneal at 900°C	1	0.16 (± 0.01)
Long anneal at 900°C	3	0.17 (± 0.01)
Long anneal at 900°C	5	0.17 (± 0.01)
Long anneal at 900°C	7	0.18 (± 0.01)
Long anneal at 900°C	10	0.20 (± 0.01)
Cyclic anneals $780/900^\circ\text{C}$	1	0.20 (± 0.01)
Cyclic anneals $780/900^\circ\text{C}$	3	0.30 (± 0.01)
Cyclic anneals $780/900^\circ\text{C}$	5	0.28 (± 0.01)
Cyclic anneals $780/900^\circ\text{C}$	7	0.23 (± 0.01)
Cyclic anneals $780/900^\circ\text{C}$	10	0.23 (± 0.01)

C. Ge/Si interdiffusion and approach to suppress interdiffusion

We have shown that the largest tensile strain is obtained when cyclic annealing is applied. This behavior can be explained due to the formation of hysteresis loops after each annealing cycle. Indeed, after growth at high temperatures followed by cooling down, the Ge layer is submitted to a certain value of the tensile strain. This implies that for the next annealing cycle, the Ge film will not behave as a perfect elastic material (note that in the case of perfect elastic materials, the stress-strain characteristic is ideally linear and the strain variation curve is perfectly superimposed over the stress variation curve). Under cyclic annealing, the Ge layer may behave visco-elastically and nonlinear behavior of stress-strain curve appears. As a consequent, the unloading curve is situated underneath the loading curve, resulting in the formation of a residual strain that increases with increasing the number of annealing cycles. However, it should be pointed out that upon annealing the strain enhancement and Ge/Si interdiffusion are competing processes. Thus, a good compromise can be obtained by controlling both the number of annealing cycles and the annealing time. It appears that the better may be to increase the number of annealing cycles while optimizing the annealing time. However, as Ge/Si interdiffusion is mainly induced during annealing at the high temperature (900°C), then the total annealing time should be taken into account (in the present case, after 10 annealing cycles 780°C (20 min)/ 900°C (20 min), the total annealing time at 900°C is 200 min). We also note that when the as-grown sample was deposited at 750°C instead of 650°C , the number of annealing cycles should be reduced in order to avoid Ge/Si interdiffusion.

To evidence the effect of Ge/Si interdiffusion with a long cyclic annealing time, we show in Fig. 11 SIMS measurements of two samples that have been annealed by 10 cycles $780/900^\circ\text{C}$: one sample corresponding to an annealing

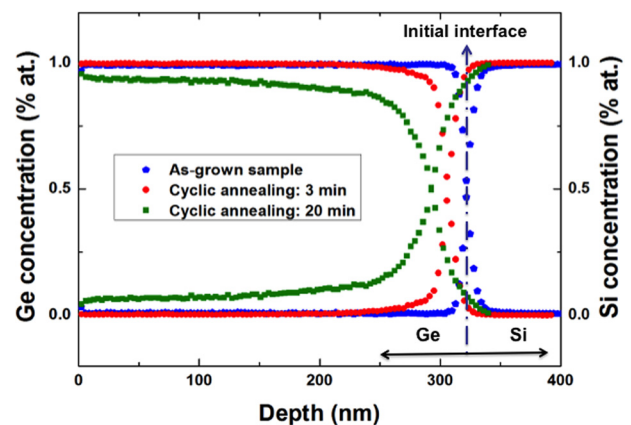


FIG. 11. SIMS profiles of the as-grown sample grown at 730°C (blue curves) and after 10 cyclic anneals at 780 and 900°C for a duration of each temperature of 3 min (red curves) and 20 min (green curves). No Ge/Si interdiffusion can be observed for the as-grown sample and after 3 min annealing, while after 20 min annealing, the deposited layer is no longer made of pure Ge but of a SiGe alloy. The Si concentration is found to continuously decrease from the interface region towards the film surface.

time of 3 min (red curves) and the other of 20 min (green curves). The growth temperature of these two samples is 730 °C. For comparison, we also show the SIMS profile of the as-grown sample (blue curves). As can be seen from the figure, the as-grown sample displays a very sharp interface, no Ge/Si interdiffusion has occurred. For the 3 min annealed sample, the evolution of both Ge and Si profiles in the deposited Ge layer does not reveal any pronounced Ge/Si interdiffusion and the deposited Ge layer remains pure. For the 20 min annealed sample, the SIMS measurements unambiguously indicate that the deposited layer is no longer made of pure Ge but of a SiGe alloy. Due to strong alloying, the interface is completely smeared out and moves toward the Ge layer. The Si concentration is not homogenous in the whole Ge layer, it is found to continuously decrease from the interface region towards the film surface.

As we have already mentioned in the introduction, one of the unique properties of Ge is the very small energy difference between its direct and indirect band gap. Thus, Si/Ge interdiffusion represents an obstacle to overcome in order to develop Ge-based optoelectronic devices. Si/Ge interdiffusion has been shown to greatly affect the optical properties of Si/Ge heterostructures³⁵ and degrade the performance of metal-oxide-semiconductor field-effect transistors (MOSFET) by reducing strain and carrier confinement and increasing alloy scattering.³⁶ To prevent interdiffusion or out-diffusion of an element, it is common to use a diffusion barrier and materials must be not only non-reactive but also are able to strongly adhere to adjacent materials. In electronic or memory devices, multilayers of metals, WN_2 , RuTiN , or RuTiO , are usually used to prevent out-diffusion of dopants (B and P) or oxidation of devices.^{37–39} Such materials are, however, difficult to insert in a heterostructure where epitaxial growth is needed. It is now generally accepted that Si and Ge atoms interdiffuse via both vacancy and interstitial-related mechanisms.⁴⁰ To prevent Si/Ge interdiffusion, in particular to suppress upward diffusion of Si to the deposited Ge layer during growth or subsequent annealing, we have experimented an approach to saturate vacancies and interstitial sites in the Ge layer near the interface region. We have chosen carbon for its small atomic radius (twice as small as Ge), carbon atoms are thus highly mobile and can easily diffuse via interstitial mechanism.^{41–43}

Fig. 12(a) shows a TEM image taken near the interface region of a sample in which we have inserted three separate carbon layers during the first step of Ge growth. Starting from a clean and (2×1) reconstructed Si surface, we first grow a 30 nm thick Ge buffer layer at 300 °C and then about 4 ML of carbon at the same temperature. Since epitaxial growth of the upper Ge layers should be conserved, the amount of deposited carbon is crucial. The latter can be determined using the change of RHEED patterns. Upon carbon deposition at 300 °C, the (2×1) RHEED pattern characteristic of a clean Ge(001) surface remains almost unchanged up to carbon coverage of 6 MLs, beyond which a faint pattern appears. Since it is crucial to insure epitaxial growth of the upper Ge layer, a carbon amount of 4 MLs is then chosen (the corresponding carbon thickness is ~ 0.3 nm). After this step, a Ge layer is deposited on top of carbon, producing therefore C/Ge stacked layers in order to increase the efficiency of carbon-induced diffusion

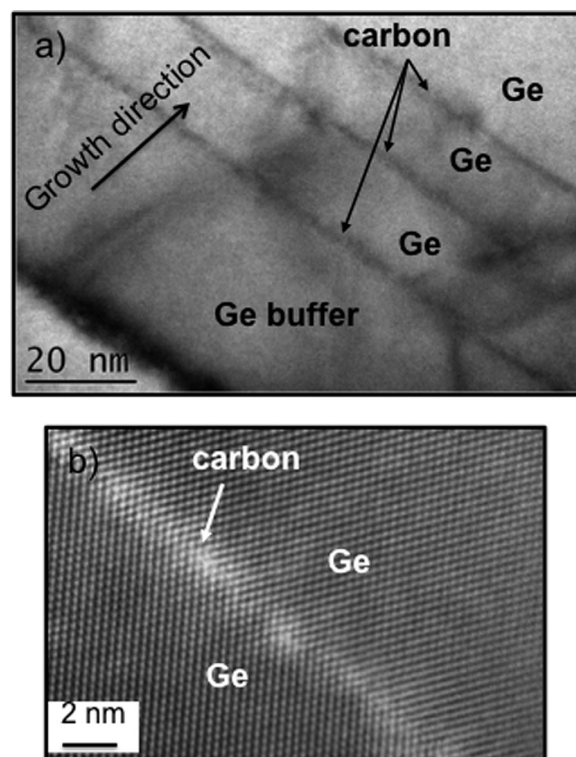


FIG. 12. (a) TEM image taken near the interface region illustrating the growth of three multilayers of C (0.3 nm)/Ge (18 nm); (b) Atomically resolved TEM image taken in the vicinity of the carbon layer. Both the underneath and the upper Ge layers are perfectly epitaxial, no presence of defects can be detected. It can be seen that carbon atoms are distributed over a distance of ~ 2 nm.

barriers. We have experimented three multilayers of C (0.3 nm)/Ge (18 nm). Fig. 12(b) shows an atomically resolved TEM image taken in the vicinity of the carbon layer. Clearly, the underneath Ge layers and also the upper Ge layers are perfectly epitaxial, without any detectable defects. The image also reveals that carbon atoms are distributed over a distance of ~ 2 nm, probably to occupy the interstitial sites of the Ge lattice or due to the strain generation arising from carbon insertion. To verify the efficiency of C/Ge multilayers to quench Si/Ge interdiffusion, we have finally grown a 300 nm thick Ge layer following the two-step growth as described previously. The high temperature step was carried out at 730 °C. After growth, the sample was cyclically annealed by 10 cycles from 780 to 900 °C and the annealing time was 20 min. In contrast to the sample shown in Fig. 11, SIMS measurements confirm that Si/Ge interdiffusion has indeed been suppressed. In Fig. 13, we display XRD measurements of two samples: one without carbon deposition (red curve) and the other containing three C/Ge multilayers. It can be clearly seen that for the sample with C/Ge multilayers the (004) diffraction order is shifted to a lower angle and at the same time the FWHM is reduced to 0.080° , a value expected for a Ge layer of the same thickness without Si/Ge interdiffusion. Finally, we note that for some samples, in particular for those exhibiting a high value of strain or a high degree of Si/Ge interdiffusion, we have also used high-resolution XRD reciprocal space mapping (RSM) around (004), (224), and $(-2-24)$ reflections to determine the strain and composition.

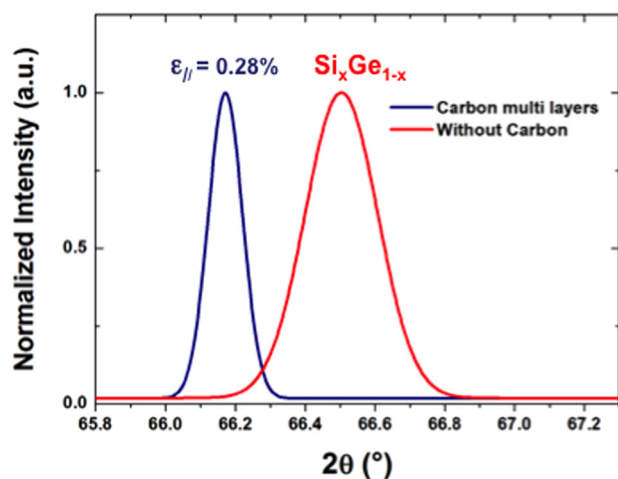


FIG. 13. Comparison of Ω - 2θ XRD scans of two samples annealed by ten 780/900 cycles during 20 min. The red curve corresponds to a sample without carbon deposition, and the blue curve corresponds to a sample containing three C/Ge multilayers deposited near the interface region. The (004) reflection of the sample with C/Ge multilayers becomes narrower and shifts to a lower angle. The corresponding tensile strain is 0.28%.

The results obtained from RSM are in good agreement with those previously reported on the tensile strain measured from XRD measurements of the symmetric (004) reflection and the film composition deduced from SIMS analysis.

IV. CONCLUSION

In summary, we have investigated the growth of tensile-strained Ge films on Si substrates using a two-step growth method by MBE. We have found that the first growth step is crucial to determine not only the film crystalline quality, the surface morphology but also the final strain state in the Ge films. We have evidenced the existence of a narrow window of the substrate temperature from 260 to 300 °C in which it is possible to completely suppress the Ge/Si Stranski-Krastanov growth. It is also shown that Ge films grown at substrate temperatures below 300 °C are metastable and that increasing the temperature leads to the generation of both misfit and threading dislocations. We have investigated the effect of both the growth temperature and annealing parameter to the strain state in the Ge films. For the growth temperature, the highest tensile strain is found to be in the range of 0.22%–0.24%, which is similar to films grown by CVD. It is also shown that cyclic annealing is more efficient than high-temperature annealing and by controlling the annealing parameter it is possible to obtain a tensile strain as high as 0.30%. To our knowledge, this value represents the highest value ever reported in the Ge/Si system. Si/Ge interdiffusion that may occur during annealing or/and growth at high temperatures appears to be the main obstacle that needs to be controlled in order to produce pure Ge-based optoelectronic devices. We have proposed an approach to use small atomic radius carbon atoms to fulfill vacancies and interstitial sites in the Ge lattice. Our results indicate that carbon incorporation seems to be a viable path to suppress Ge/Si interdiffusion.

ACKNOWLEDGMENTS

This work was supported by the French ANR Program via the GRAAL project (Blanc 2011 BS03 004 01) and partially supported by the JSPS Core-to-Core Program, Advanced Research Networks “International Collaborative Research Center on Atomically Controlled Processing for Ultralarge Scale Integration.”

- ¹J. Liu, X. Sun, R. Camacho-Aguilera, L. C. Kimerling, and J. Michel, *Opt. Lett.* **35**, 679 (2010) and references therein.
- ²J. Liu, X. Sun, D. Pan, X. Wang, L. C. Kimerling, T. L. Koch, and J. Michel, *Opt. Exp.* **15**, 11272 (2007).
- ³M. El Kurdi, G. Fishman, S. Sauvage, and P. Boucaud, *J. Appl. Phys.* **107**, 013710 (2010).
- ⁴X. Sun, J. F. Liu, L. C. Kimerling, and J. Michel, *Appl. Phys. Lett.* **95**, 011911 (2009).
- ⁵M. El Kurdi, T. Kociniowski, T.-P. Ngo, J. Boulmer, D. Débarre, P. Boucaud, J. F. Damlencourt, O. Kermarrec, and D. Bensahel, *Appl. Phys. Lett.* **94**, 191107 (2009).
- ⁶M. El Kurdi, H. Bertin, E. Martincic, M. de Kersauson, G. Fishman, S. Sauvage, A. Bosseboeuf, and P. Boucaud, *Appl. Phys. Lett.* **96**, 041909 (2010).
- ⁷Y. Bai, K. E. Lee, C. Cheng, M. L. Lee, and E. A. Fitzgerald, *J. Appl. Phys.* **104**, 084518 (2008).
- ⁸R. Jakomin, M. de Kersauson, M. El Kurdi, L. Largeau, O. Mauguin, G. Beaudoin, S. Sauvage, R. Ossikovski, G. Ndong, M. Chaigneau, I. Sagnes, and P. Boucaud, *Appl. Phys. Lett.* **98**, 091901 (2011).
- ⁹Y.-Y. Fang, J. Tolle, R. Roucka, A. V. G. Chizmeshya, J. Kouvetakis, V. R. D’Costa, and J. Menéndez, *Appl. Phys. Lett.* **90**, 061915 (2007); J. Menéndez and J. Kouvetakis, *ibid.* **85**, 1175 (2004).
- ¹⁰S. Takeuchi, Y. Shimura, O. Nakatsuka, S. Zaima, M. Ogawa, and A. Sakai, *Appl. Phys. Lett.* **92**, 231916 (2008).
- ¹¹Y. Ishikawa and K. Wada, *Thin Solid Films* **518**, S83 (2010).
- ¹²See, for example, and references therein, J. Liu, R. Camacho-Aguilera, J. T. Bessette, X. Sun, X. Wang, Y. Cai, L. C. Kimerling, and J. Michel, *Thin Solid Films* **520**, 3354 (2012).
- ¹³J. Werner, M. Oehme, M. Schmid, M. Kaschel, A. Schirmer, E. Kasper, and J. Schulze, *Appl. Phys. Lett.* **98**, 061108 (2011).
- ¹⁴E. Kasper, M. Oehme, J. Werner, T. Aguirov, and M. Kittler, *Front. Optoelectron.* **5**, 256 (2012).
- ¹⁵M. Oehme, M. Gollhofer, D. Widmann, M. Schmid, M. Kaschel, E. Kasper, and J. Schulze, *Opt. Exp.* **21**, 2206 (2013).
- ¹⁶D. J. Eaglesham and M. Cerullo, *Phys. Rev. Lett.* **64**, 1943 (1990).
- ¹⁷V. Le Thanh, *Surf. Sci.* **492**, 255 (2001) and references therein.
- ¹⁸L. Colace, G. Masini, F. Galluzzi, G. Assanto, G. Capellini, L. Di Gaspare, E. Pelange, and F. Evangelisti, *Appl. Phys. Lett.* **72**, 3175 (1998).
- ¹⁹H.-C. Luan, D. R. Lim, K. K. Lee, K. M. Chen, J. G. Sandland, K. Wada, and L. C. Kimerling, *Appl. Phys. Lett.* **75**, 2909 (1999).
- ²⁰J.-M. Hartmann, A. Abbadie, A. M. Papon, P. Holliger, G. Rolland, T. Billon, J. M. Fédéli, M. Rouvière, L. Vivien, and S. Laval, *J. Appl. Phys.* **95**, 5905 (2004).
- ²¹J.-M. Hartmann, A. M. Papon, V. Destefanis, and T. Billon, *J. Cryst. Growth* **310**, 5287 (2008).
- ²²B. S. Meyerson, *IBM J. Res. Develop.* **44**, 132 (2000).
- ²³V. Le Thanh, V. Aubry-Fortuna, Y. Zheng, D. Bouchier, C. Guedj, and G. Hincelin, *Thin Solid Films* **294**, 59 (1997).
- ²⁴V. Le Thanh, V. Aubry-Fortuna, D. Bouchier, A. Younsi, and G. Hincelin, *Surf. Sci.* **369**, 85 (1996).
- ²⁵M. Halbax, D. Bouchier, V. Yam, D. Débarre, Lam H. Nguyen, Y. Zheng, P. Rosner, M. Benamara, H. P. Strunk, and C. Clerc, *J. Appl. Phys.* **97**, 064907 (2005).
- ²⁶M. Stoffel, L. Simon, J. L. Bischoff, D. Aubel, L. Kubler, and G. Castelein, *Thin Solid Films* **380**, 32 (2000).
- ²⁷V. Le Thanh, D. Bouchier, and G. Hincelin, *J. Appl. Phys.* **87**, 3700 (2000).
- ²⁸P. M. Mooney, F. K. LeGoues, and J. L. Jordan-Sweet, *Appl. Phys. Lett.* **65**, 2845 (1994).
- ²⁹M. G. Lagally, in *Method of Experimental Physics*, Vol. 22, Solid State Physics: Surfaces, edited by R. L. Park and M. G. Lagally (Academic, New York, 1985).
- ³⁰J. Liu, H. J. Kim, O. Hul’ko, Y. H. Xie, S. Sahni, P. Bandaru, and E. Yablonovitch, *J. Appl. Phys.* **96**, 916 (2004).

- ³¹J. Liu, D. D. Cannon, Y. Ishikawa, K. Wada, D. T. Danielson, S. Jongthammanurak, J. Michel, and L. C. Kimerling, *Phys. Rev. B* **70**, 155309 (2004).
- ³²L. Souriau, T. Atanasova, V. Terzieva, A. Moussa, M. Caymax, R. Loo, M. Meuris, and W. Vandervorst, *J. Electrochem. Soc.* **155**, H677 (2008).
- ³³M. A. Lutz, R. M. Feenstra, F. K. LeGoues, P. M. Mooney, and J. O. Chu, *Appl. Phys. Lett.* **66**, 724 (1995).
- ³⁴M. Albrecht, S. Christiansen, J. Michler, W. Dorsch, H. P. Strunk, P. O. Hansson, and E. Bauser, *Appl. Phys. Lett.* **67**, 1232 (1995).
- ³⁵P. Boucaud, L. Wu, C. Guedj, F. H. Julien, I. Sagnes, Y. Campidelli, and L. Garchery, *J. Appl. Phys.* **80**, 1414 (1996).
- ³⁶J. Jung, S. F. Yu, O. O. Olubuyide, J. L. Hoyt, D. A. Antoniadis, M. L. Lee, and E. A. Fitzgerald, *Appl. Phys. Lett.* **84**, 3319 (2004).
- ³⁷D.-S. Yoon, J. S. Roh, S.-M. Lee, and H. K. Baik, *Prog. Mater. Sci.* **48**, 275 (2003).
- ³⁸S. Becker and R. G. Gordon, *Appl. Phys. Lett.* **82**, 2239 (2003).
- ³⁹C. Y. Ting, *Thin Solid Films* **119**, 11 (1984).
- ⁴⁰Y. Dong, Y. Lin, S. Li, S. McCoy, and G. Xia, *J. Appl. Phys.* **111**, 044909 (2012).
- ⁴¹A. Spiesser, I. Slipukhina, T. Dau, E. Arras, V. Le Thanh, L. Michez, P. Pochet, H. Saito, S. Yuasa, M. Jamet, and J. Derrien, *Phys. Rev. B* **84**, 165203 (2011).
- ⁴²M. T. Dau, V. Le Thanh, T. G. Le, A. Spiesser, M. Petit, L. A. Michez, and R. Daineche, *Appl. Phys. Lett.* **99**, 151908 (2011).
- ⁴³M. T. Dau, V. Le Thanh, T. G. Le, A. Spiesser, M. Petit, L. A. Michez, T. H. Ngo, D. L. Vu, Q. L. Nguyen, and P. Sebban, *Thin Solid Films* **520**, 3410 (2012).